Nonwetting Behavior of Al–Co Quasicrystalline Approximants Owing to Their Unique Electronic Structures

Kanika Anand, Vincent Fournée, Geoffroy Prévot, Julian Ledieu, and Émilie Gaudry*

ABSTRACT: Good wetting is generally observed for liquid metals on metallic substrates, while poor wetting usually occurs for metals on insulating oxides. In this work, we report unexpected large contact angles for lead on two metallic approximants to decagonal quasicrystals, namely, Al_5Co_2 and $Al_{13}Co_4$. Intrinsic surface wettability is predicted from first principles, using a thermodynamic model based on the Young equation, and validated by the good agreement with experimental measurements performed under ultra-high vacuum by scanning electron microscopy. The atomistic details of the atomic and electronic structures at the Pb-substrate interface, and the comparison with Pb(111)/Al(111), underline the influence of the specific electronic structures of quasicrystalline approximants on wetting. Our work suggests a possible correlation of the contact angles with the density of states at the Fermi energy and paves the way for a better fundamental understanding of wettability on intermetallic substrates, which has potential consequences in several applications such as supported catalysts, protective coatings, or crystal growth.

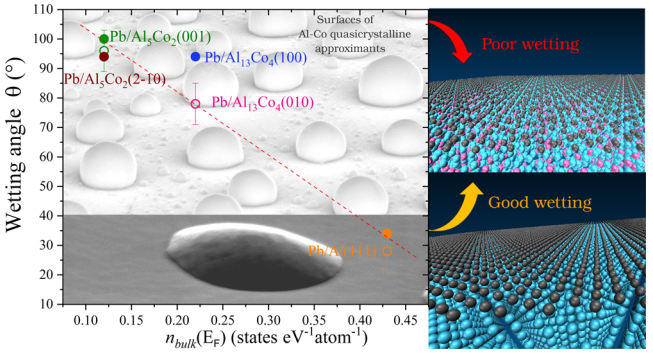

KEYWORDS: *wetting, contact angle, interfacial energy, quasicrystalline approximant surfaces, electronic structures, scanning electron microscopy, density functional theory*

1. INTRODUCTION

The design of metallic alloys with specific wetting properties is crucial for numerous technological applications. Efficient hydrophobic attributes are required for anti-icing surfaces,[1−4] self-cleaning materials,[5−7] or corrosion-resistant layers.[4,8,9] The way a liquid wets a solid is also decisive for crystal growths,[10,11] solidification processes,[12,13] or joining technologies.[14] For some applications, the targeted wetting characteristics can be achieved artificially by the preparation of surfaces with complex textures and architectures[15,16] or by the deposition of molecular layers with specific properties.[17,18] Much less efforts have focused on the development of metallic alloys with specific intrinsic wetting properties.

Wetting properties are quantified through contact angles, that is, angles where a liquid−vapor interface meets a solid surface. For nonreactive metal liquids on solids, the intrinsic contact angles result from two types of competing forces: adhesion forces between the liquid and the solid phases and cohesion forces of the liquid.[19] Then, in the absence of barriers to wetting such as oxide films, good wetting, that is, contact angles of a few degrees or tens of degrees, is observed if the interactions occurring at the interface are significant. This is fulfilled for liquid metals on metallic substrates because in this type of systems, the interfacial bond is strong (metallic).[20]

Unexpected large contact angles have been measured for several liquids deposited on Al-based quasicrystalline alloys, that is, intermetallic compounds characterized by a long-range atomic order with no periodicity.[21,22] In these experiments, the substrates were however covered by a very thin surface layer of alumina oxide, which avoided the determination of their intrinsic wetting properties. The outstanding values of the contact angles were then attributed to a combination of intrinsic and extrinsic factors, namely, the specific electronic density of states within the bulk material, underneath the oxide layer, and thickness of the oxide layer.

A few attempts have been carried out to disentangle the intrinsic contributions of the Al-based quasicrystalline substrate from those of the oxide layer.[23,24] From the experimental point of view, such a goal is challenging. It requires ultra-high vacuum (UHV) conditions and a careful preparation of the system: deposition of a metal thin film on a clean surface free from any contaminants, in situ dewetting

https://dx.doi.org/10.1021/acsami.9b20653

leading to the formation of droplets, and determination of the contact angle using Scanning Electron Microscopy (SEM). On the other hand, intrinsic wetting properties of quasicrystalline surfaces can be determined through theoretical calculations based on the droplet method or on free-energy calculations. Such approaches have been widely used to determine contact angles and interfacial energies of a large variety of systems.[25−27] However, in most cases, the simulations largely rely on classical potentials. This may lead to interfacial energies (γ) and contact angles (θ) significantly different from the ones determined experimentally, even for simple systems such as Pb(111)/Al(111)—$\gamma^{calc}_{Pb/Al(111)}$ = 28.3 meV/Å^2 ($\gamma^{exp}_{Pb(111)/Al(111)}$ = 13.5 ± 2 meV/Å^2)[28,29] and $\theta^{calc}_{Pb/Al}$ = 46.4° ($\theta^{exp}_{Pb/Al(111)}$ = 27.3 ± 0.8°)[28,30]—which questions the possibility of assessing accurate values of contact angles from classical potentials which do not explicitly consider electronic effects.

In this work, using liquid lead as a probe, we identify notable intrinsic low wetting behaviors, that is, contact angles close to or larger than 90°, for two intermetallic substrates considered as approximants to decagonal quasicrystals, namely, Al_5Co_2 and $Al_{13}Co_4$. A quantitative and predictive method to evaluate the intrinsic contact angles, applicable to a broad range of intermetallic substrates and validated by the good agreement with a few experimental measurements, is proposed based on the Young equation combined with density functional theory (DFT). Electronic effects are found to have a significant influence on the wetting properties of the considered quasicrystalline-related substrates. Our study suggests a possible correlation of the contact angles with the density of states at the Fermi energy. It opens a way to design intermetallic alloys with targeted wetting properties based on this factor.

2. MATERIALS AND METHODS

2.1. Experimental Details. The two approximant substrates used in this study were extracted from single crystals grown by the Czochralski technique, as detailed in ref 31 for Al_5Co_2 and in ref 32 for $Al_{13}Co_4$. The $Al_{13}Co_4$(010) and Al_5Co_2(001) surfaces were prepared under UHV (base pressure of 2 × 10^{-10} mbar) by repeated cycles of Ar^+ sputtering and annealing, as described in refs 31 and 33. The structures of the clean surfaces were checked by low-energy electron diffraction prior to Pb deposition.

Lead was then dosed on the clean surfaces for a few minutes using a Knudsen cell to form a thick uniform layer on the substrates. The pressure was kept in the low 10^{-9} mbar range during deposition. Samples were further heated slightly above the melting point of Pb (T = 357 °C, T^{Pb}_m = 327 °C) to produce liquid droplets of micrometer size or smaller. The temperature was then decreased gradually to room temperature.

Auger spectra in between the droplets indicate the presence of some O contamination and the presence of a Pb wetting layer still covering the substrate after the formation of the droplets, in agreement with previous observations (Figure S1).[28] Contact angles were further determined from in situ SEM imaging at room temperature, with a tilt angle between the surface normal and the in-lens secondary electron detector up to 70° (NanoSEM/SAM, ScientaOmicron). High resolution micrographs were analyzed by means of standard ImageJ software, based on a circular-curve fitting (Table S1 and Figure S2).

2.2. Computational Details. All calculations are based on DFT and use the Vienna ab Initio Simulation Package (VASP). Self-consistent Kohn Sham equations were solved by means of the projected-augmented wave method.[34,35] Atomic structures were relaxed using the conjugate gradient method until the forces are lower than 0.02 eV/Å. The considered systems were modeled with p-layer thick slabs separated by a void thickness equal to 15 Å (p = 6 for $Al_5Co_2(2\bar{1}0)$, p = 7 for Al_5Co_2(001) and $Al_{13}Co_4$(100) and p = 9 for Al(111)). The plane-waves energy cut-off was set to 450 eV. Monkhorst−Pack meshes were used for the k-points sampling:[36] 5 × 5 × 1 for Pb/Al(111) (Moiré structure), 1 × 7 × 7 for Pb/$Al_{13}Co_4$(100), 7 × 7 × 1 for Pb/Al_5Co_2(001) and 1 × 3 × 11 for Pb/$Al_5Co_2(2\bar{1}0)$. Finer k-point grids were used for density of states calculations. Our approach adopts the standard semilocal PBE functional.[37,38] Within this approximation, cell parameters, cohesive energies of bulk systems as well as surface energies of oriented crystals are in good agreement with the literature[39−41] (Tables S2 and S3).

2.3. Bulk and Clean Surface Structures. The Al_5Co_2 and $Al_{13}Co_4$ compounds crystallize in the $P6_3/mmc$ (no. 194, hP28)[42] and $Pmn2_1$ (no. 31, oP102)[43] space groups, respectively. Both structures can be described by a stacking of two types of layers (either flat or corrugated layer), that is, alternate perpendicular to [100] for $Al_{13}Co_4$ and perpendicular to $[2\bar{1}0]$ and [001] for Al_5Co_2 (Figure S3).

The clean surface structures have been deduced from a combination of surface science studies under UHV and theoretical calculations.[31,33,44−46] The two considered low index surface structures of Al_5Co_2 arise from surface termination at incomplete puckered layers with specific atomic arrangements missing, thus forming reconstructions (Figure 1). The $Al_{13}Co_4$(100) surface structure from a plane selection and consists of dense Al-rich layers with the surface Co atom missing (Figure 1).[33,45,46] In all cases, the termination layer is Al-rich, and the average terrace size is of the order of 0.1 μm, as observed by scanning tunneling microscopy (STM).

2.4. Interfaces: Thermodynamic Approach and Structural Models. Two types of simulation methods are generally used to determine contact angles.[47] Similar to the experimental approach, the droplet method consists in considering a liquid droplet on a surface. When a well-defined shape is obtained by simulations, the contact angle is calculated. The previous method may however suffer from finite size effects (line tension, interfacial curvature, or arbitrary choice of the solid-fluid contact plane). Methods based on free energy calculations are not as straightforward as the droplet simulations but tend to provide more accurate contact angle estimates.[48]

Here, the contact angles are determined through the Young equation (Figure 2),[49,50] which involves surface ($\gamma^{substrate}$) and interfacial ($\gamma^{interface}$) energies

$$\cos\theta = \frac{\gamma^{substrate} - \gamma^{interface}}{\gamma^{Pb}} \quad (1)$$

The surface energy of lead in the previous equation is taken to be the one of Pb(111) ($\gamma_{Pb} = \gamma_{Pb(111)}$). This assumption is supported by the temperature at which the experimental measurements were performed (Pb is solid at room temperature) and by the similar surface energies and electronic structures of dense liquid and fcc Pb.[51−53]

According to the scheme shown in Figure 2, the interfacial energy is given by

$$\gamma^{interface} = \frac{E^{tot}_{system} - A \times (\gamma^{Pb(111)} + \gamma^{substrate}) - \sum_X n_X \times \mu^X}{A} \quad (2)$$

where E^{tot}_{system}, μ^X, $\gamma^{substrate}$, $\gamma^{Pb(111)}$, n_X, and A are the total energy of the considered system, the chemical potentials of the X species (X = Pb, Co, and Al), the surface energy of the substrate (Tables S2, S3 and 2), the surface energy of Pb(111) (17.8 meV/Å^2), the number of X atoms in the system, and the interfacial area, respectively. Because the intermetallic compounds are synthesized from an Al-rich melt, the Al chemical potential is taken as the one of bulk Al in the previous equations ($\gamma^{substrate}$, μ^X).

Experimentally, lead is observed in between the Pb droplets. The surface energy of the substrate has then to be corrected from Pb adsorption, as already shown by ref 28

$$\gamma^{substrate}_{modified} = \gamma^{substrate} + \frac{E_{ads}}{A}$$
$$\text{with } E_{ads} = E^{tot}_{slab+1\ Pb\text{-}layer} - E^{tot}_{substrate} - n_{Pb} \times E^{Pb}_{coh} \quad (3)$$

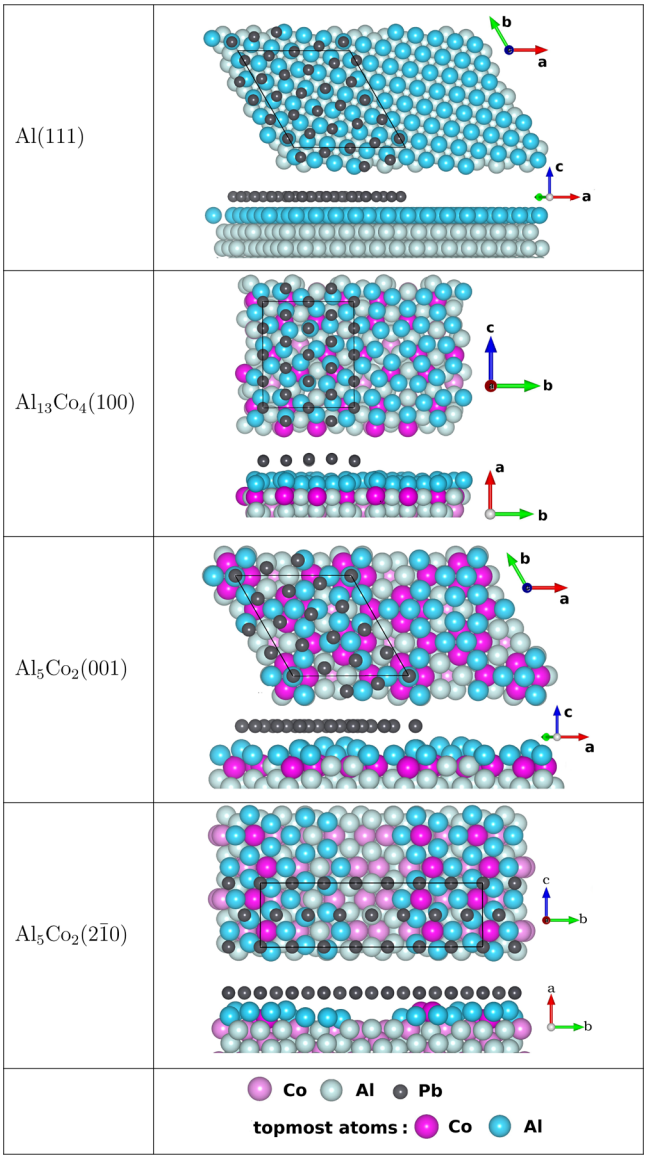

Figure 1. Structures of the Al(111), $Al_{13}Co_4(100)$, $Al_5Co_2(001)$, and $Al_5Co_2(2\bar{1}0)$ surfaces, along with the corresponding lead interfaces (before structural relaxation).

where $E^{tot}_{slab+1Pb\text{-}layer}$, $E^{tot}_{substrate}$, and E^{Pb}_{coh} are the total energies of the substrate covered with a Pb atomic layer, the total energy of the clean substrate, and the lead cohesive energy ($E^{Pb}_{coh} = \mu^{Pb}$).

The previous approach is based on slab models, built with a substrate covered by n-layer thick dense Pb(111) films (hexagonal-like models), with $1 \leq n \leq 4$. For Pb(111)/Al(111), we considered a $(\sqrt{31} \times \sqrt{31})R8.95°$ higher-order commensurate structure relative to Al(111), corresponding to a $(\sqrt{21} \times \sqrt{21})R10.9°$ reconstruction of Pb(111) (lattice parameter 15.9 Å), in agreement with the experimental observations[54] (Figure 1), as illustrated by the comparison of the simulated and experimental STM images (Figure S4). The other interfaces have been built in order to minimize the lattice mismatch between Pb(111) and the considered substrate. It leads to a $(\sqrt{13} \times \sqrt{13})R13.9°$ reconstruction of Pb(111) for Pb/$Al_5Co_2(001)$, a $\begin{pmatrix} 7 & 1 \\ 0 & 2 \end{pmatrix}$ superstructure of Pb(111) for Pb/$Al_5Co_2(2\bar{1}0)$, and a $\begin{pmatrix} 4 & 0 \\ 2 & 4 \end{pmatrix}$ superstructure of Pb(111) for Pb/$Al_{13}Co_4(100)$ (5, 7, and 2.5% averaged lattice mismatches, respectively).

For Pb/$Al_{13}Co_4(100)$, in addition to the previous hexagonal-like Pb adlayer models, we considered a 1-layer thick Pb adlayer slab built by progressively filling all favorable adsorption sites.[55] The corresponding modified surface energy ($\gamma^{substrate}_{modified}$) calculated as a function of the Pb coverage presents a discontinuity for a coverage equal to 0.090 at./Å^2 (Figure 3): the modified surface energy

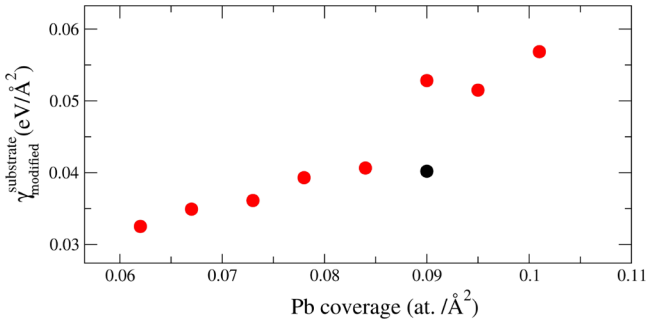

Figure 3. Modified surface energy of $Al_{13}Co_4(100)$, considering Pb atoms adsorbed at the surface, in the favorable adsorption sites identified in refs 56 and 57 (single Pb layer, in red). The black points correspond to a "bilayer" structure (15 + 1 Pb atoms/ surf. cell).

increases abruptly, becoming larger than the one of a lead bilayer (15 + 1 at./surf. cell). This supports an optimal coverage equal to 15 atoms per cell for a single Pb adlayer, in good agreement with the Pb coverage observed experimentally (0.090 at./Å^2).[56] This structural model was used to build a 4-layer thick Pb adlayer slab, where the two first adlayers are pseudomorphic (15 Pb atoms/surface cell) and the other two Pb adlayers are dense (16 Pb atoms/surface cell). We will refer to this model as the pseudomorphic-like Pb adlayer model.

Finally, for Pb/$Al_{13}Co_4(100)$, models have also been built using interfacial structures derived from ab initio molecular dynamic (AIMD) simulations carried out in the canonical ensemble (total simulation time of runs = 50 ps, timestep = 1 fs, $T = T^{Pb}_m$ = 600 K), followed by a DFT-based conjugate-gradient structure optimization. We took simulation cells containing a 7-layer thick $Al_{13}Co_4(100)$ slab topped with a 6 Å thick region filled with lead. The resulting structure was used to build 4-layer thick Pb adlayer slabs (the first two Pb adlayers come from AIMD, and the other two Pb adlayers are dense layers). We will refer to this model as the MD-like Pb adlayer model.

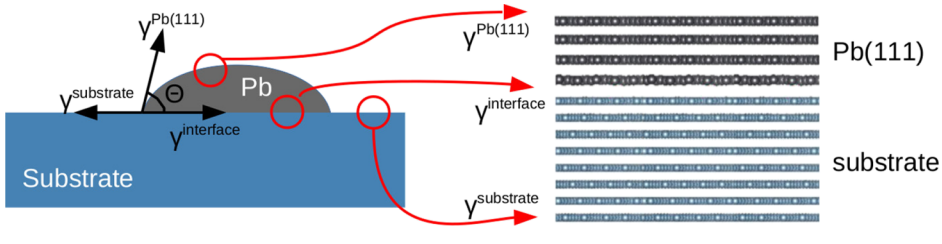

Figure 2. Schematic diagram to predict the surface wettability of Al-based approximants by lead. Surface energies of the substrate and lead are calculated separately and used in eqs 1 and 2 to evaluate the interfacial energy (DFT slab model, right-hand side).

3. RESULTS

3.1. Contact Angles. Contact angles are experimentally measured for Pb/Al(111), Pb/$Al_{13}Co_4$(010), and Pb/Al_5Co_2(001) (Table 1 and Figure 4), avoiding points very close to any crystal facet, as it would lead to misleading contact angles. The shape of the Pb droplets are typically spherical after liquid dewetting, with eventually small flat facets in narrow regions attributed to the small anisotropy of the Pb surface energy. A nonwetting behavior is observed for Pb/Al_5Co_2(001) and Pb/$Al_{13}Co_4$(010), with contact angles of 96 ± 7 and 78 ± 7°, respectively, demonstrating the specific intrinsic wetting properties of the quasicrystalline approximant.

Table 1. Experimental (θ^{exp}) and Theoretical (θ^{calc}) Contact Angles for Pb Droplets on Different Substrates (Hexagonal-like Structures), along with the Density of States ($n_{bulk}(E_F)$) at the Fermi Energy, Resulting from DFT Calculations

substrate	θ^{exp} (deg)	θ^{calc} (deg)	n_{bulk} (E_F) (states/(eV·atom))
Al(111)	28 ± 7	35	0.43
Al_5Co_2(001)	96 ± 7	100	0.12[31]
$Al_5Co_2(2\bar{1}0)$		94 (68[a])	0.12[31]
$Al_{13}Co_4$(010)	78 ± 7		0.22
$Al_{13}Co_4$(100)		94 (82[b], 116[c])	0.22

[a]The value for the $P_{B\text{-}4Co}$ model (see Table S3). [b]The value for the pseudomorphic-like structures (see text). [c]The value for the MD-like structures (see text)

According to our thermodynamic model, the contact angles calculated for Pb/Al(111), Pb/Al_5Co_2(001), Pb/$Al_5Co_2(2\bar{1}0)$, and Pb/$Al_{13}Co_4$(100) are 35, 100, 94, and 94°, respectively, using hexagonal-like four layers models (Table 1). These values match our experimental observations when available, assessing the validity of our theoretical approach. For Pb(111)/$Al_{13}Co_4$(100), our theoretical value is rather different from the value published in ref 24 (45°). Such discrepancy is attributed to the differences between the experimental and theoretical substrates. The calculation considered the single crystalline $Al_{13}Co_4$(100) homogeneous surface, while the experimental study of ref 24 relies on a polycrystalline thin film prepared by evaporation of Al/Co multilayers followed by an appropriate annealing treatment, the nominal Al/Co atomic ratio of the sample corresponding to 13:4 on average. Such surface probably presents increased roughness as well as both structural and chemical heterogeneity compared to the homogeneous single crystal (100) surface considered in the calculations. In addition, the theoretical contact angle determined on the (100) surface is on the same order of magnitude as the experimental angle measured for the Pb/$Al_{13}Co_4$(010) system,[58] which reinforces the reliability of our prediction, the anisotropy of the contact angles being assumed to be small (see Discussion section).

3.2. Interfacial Energies and Electronic Structures. The theoretical interfacial energies are gathered in Table 2. For Pb(111)/Al(111), they are almost the same for all considered Pb adlayer thicknesses, in agreement with the layer-by-layer growth of thick Al films described in ref 54. The situation is different in the case of the Al/Co quasicrystalline approximants. Here, the interfacial energy sharply increases from one to two Pb adlayers and remains almost the same for three and four Pb adlayers. It shows an energetic cost for the growth of Pb thick films on such substrates. For Pb/$Al_{13}Co_4$(100), this is in agreement with the experimental finding that Pb thin films do not grow in a layer-by-layer fashion on that surface.[56]

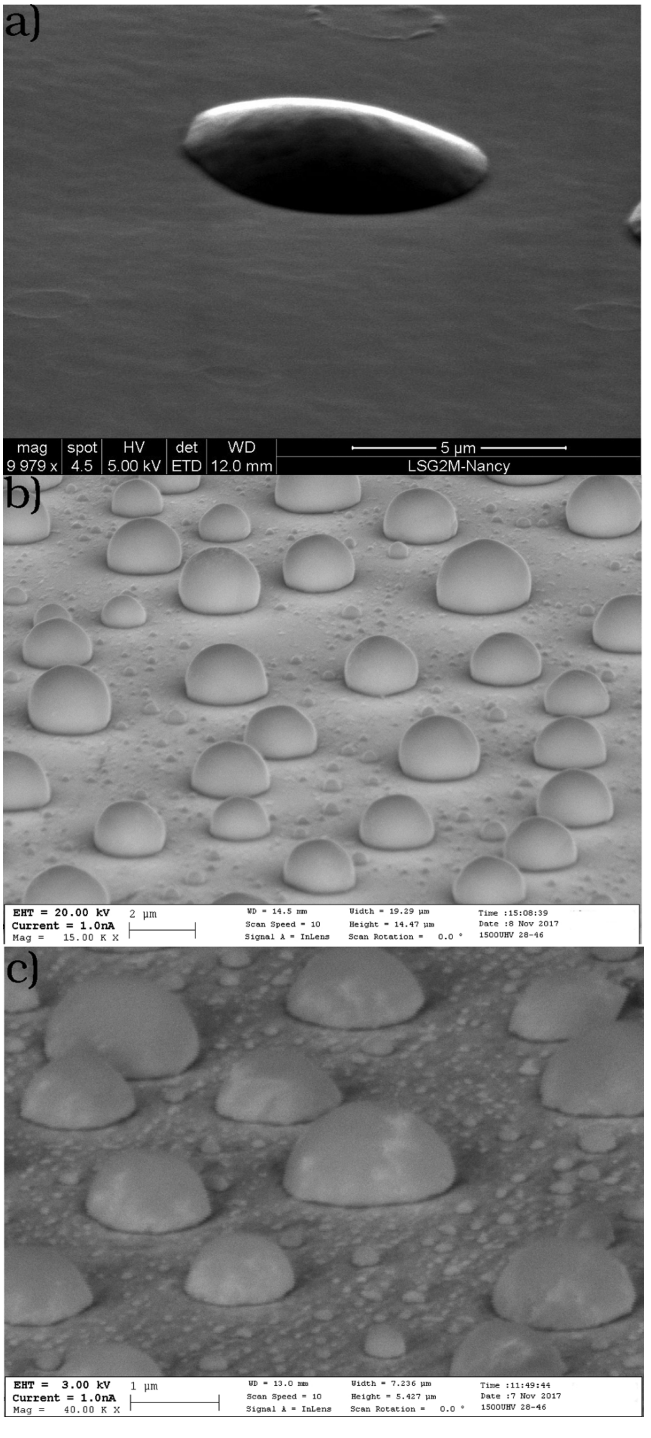

Figure 4. SEM micrographs showing Pb droplets on (a) Al(111), (b) Al_5Co_2(001), and (c) $Al_{13}Co_4$(010).

Interfacial Pb electronic structures are shown in Figure 5 and Figure S5 for different systems. They are compared to the ones of bulk Pb and of a freestanding Pb(111) single layer. The s and p bands of Pb bulk DOS extend over the [−11.5; −6.75 eV] region and from −4 eV. Such separation of the s and p states, observed in the bulk DOS, also occurs in the freestanding Pb single layer because it is not structure induced.[52,59] This feature does not appear anymore for Pb deposited on the different substrates, probing the interaction of

Table 2. Surface Energies ($\gamma^{substrate}$, meV/Å^2), Modified Surface Energies ($\gamma^{substrate}_{modified}$, meV/Å^2), Work Functions ($W^{substrate}$, eV) for Clean Surfaces, and Interfacial Energies ($\gamma_n^{interface}$, meV/Å^2) as a Function of the Pb Adlayer Thickness ($n \in \{1, 2, 3, 4\}$) for the Al(111), $Al_5Co_2(001)$, $Al_5Co_2(2\bar{1}0)$, and $Al_{13}Co_4(100)$ Substrates (Hexagonal-like Models)

	Al(111)	$Al_{13}Co_4(100)$	$Al_5Co_2(001)$	$Al_5Co_2(2\bar{1}0)$
$\gamma^{substrate}$	50.1	65.6	83.8	87.6
$\gamma^{substrate}_{modified}$	37.6	40.9	55.2	55.4
$W^{substrate}$	3.85	4.26	4.02	4.37
$\gamma_1^{interface}$	19.7	23.1	37.4	37.7
$\gamma_2^{interface}$	22.1	37.6	55.6	54.7
$\gamma_3^{interface}$	23.4	32.2	57.7	58.6
$\gamma_4^{interface}$	23.0 (18.5[a])	42.3	58.3	56.7

[a]The value obtained for the Pb(111)/Al(111) interface using a slab which does not contain any vacuum layer.

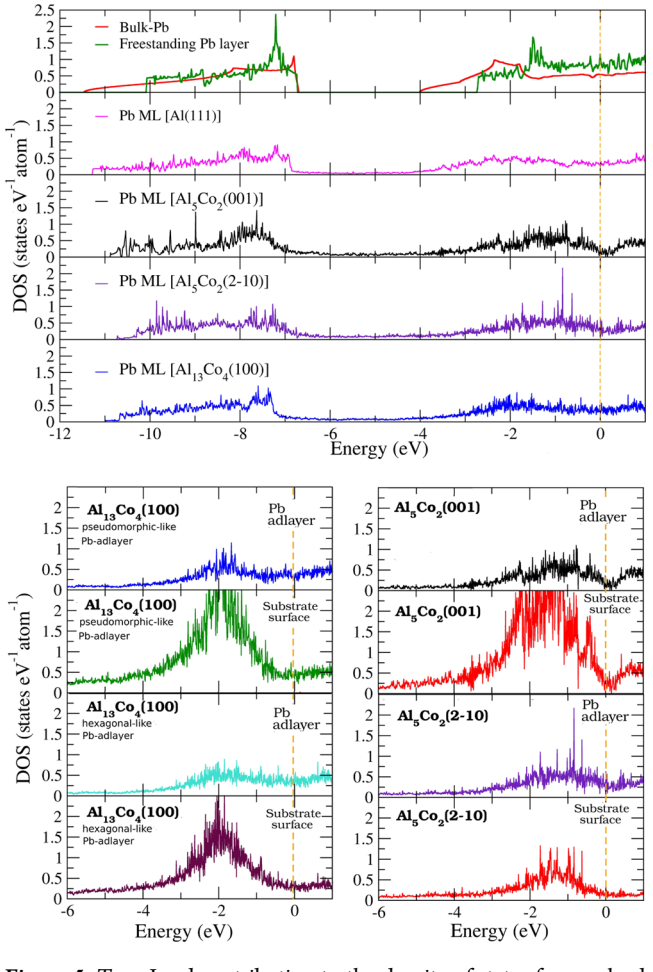

Figure 5. Top: Lead contribution to the density of states for one lead monolayer deposited on Al(111), $Al_5Co_2(001)$, $Al_5Co_2(2\bar{1}0)$, and $Al_{13}Co_4(100)$. DOS of a freestanding Pb layer and the DOS of bulk Pb are given for comparison. Bottom: Contributions to the DOS from the surface layers of the $Al_{13}Co_4(100)$ and $Al_5Co_2(001)$ substrates and from the first Pb adlayer. The interfacial structure is based on the hexagonal-like Pb adlayer structure for $Al_{13}Co_4(100)$, $Al_5Co_2(2\bar{1}0)$, and $Al_5Co_2(001)$. For $Al_{13}Co_4(100)$, we also considered the pseudomorphic-like structure.

Pb states with the substrate Al states. For Al/Co compounds, a larger interaction is noticeable around −2 eV because of hybridization with the Co d-states. The contribution of Pb atoms to the DOS of $Pb(111)/Al_5Co_2(001)$ exhibits a clear and faint minimum at the Fermi energy (called the pseudogap, Figure 5). The pseudogap is present for the clean $Al_5Co_2(2\bar{1}0)$ and $Al_{13}Co_4(100)$ surfaces but not visible when hexagonal- or pseudomorphic-like Pb adlayers are present (Figure 5).

4. DISCUSSION

In this work, we determined interfacial energies for Pb/Al and Pb/Al−Co compounds as a function of the Pb film thickness in the range from one to four layers. For Pb(111)/Al(111), our result (23.0 meV/Å^2) is in better agreement with the experimental value (13.5 meV/Å^2)[28] than the one of a previous theoretical study (28.3 meV/Å^2).[29] The interfacial structure considered in ref 29 was a Moiré structure as well but different from the one determined experimentally. In addition, the modeling was based on empirical potentials and did not consider any vacuum layer, avoiding the consideration of the lead surface energy. Using the same approach but with the experimental Moiré structure and DFT-based calculations, we obtained an interfacial energy equal to 18.5 meV/Å^2. The accuracies achieved on interfacial energies, leading to the determination of contact angles in good agreement with the experimental measurements, are due to the consideration of electronic effects on wetting. For Pb(111)/Al(111) with the model of hexagonal layers, we determine a contact angle equal to 35°, in good agreement with the experimental value (28 ± 7°), while molecular dynamics calculations based on empirical potentials led to a higher value (46.4°).[30] Besides electronic effects, the consideration of surface energies in our model is essential. Methods based on adsorption energies only,[48,60,61] although they appear well adapted for the determination of water-wetting properties, seems not to be adequate for the determination of wetting properties using a metal as a probe.

The previous example shows that the interface is crucial to determine the wetting properties. The consideration of a realistic structure for the first lead atomic layer on the substrate is important. Contact angles may be overestimated if the lowest energy configuration for the interface is not reached. In this work, we considered dense Pb adlayers, with an interface built either on the basis of experimental observations (Pb(111)/Al(111)) or driven by the minimization of the lattice mismatch between the substrate and Pb(111). A rough estimation of the influence of the interface on contact angles was carried out for $Pb/Al_{13}Co_4(100)$. Several interfacial structures were considered: hexagonal-like, pseudomorphic-like, and MD-like. While results of the same order of magnitude were found for contact angles (94, 82, and 116°, Tables S3 and S4), the lowest contact angle was determined in the case of the pseudomorphic-like structure, that is, the more realistic one (a pseudomorphic growth was observed experimentally[56]). Our results using the hexagonal-like structure are not so different—they can be considered as acceptable. It is attributed to the balance arising from the adlayer−substrate interaction strength and from the adlayer atomic density (16 and 15 atoms per surface cell for the hexagonal-like and pseudomorphic-like structures, respectively).

The previous observations suggest that the aperiodic or periodic nature of the interface may influence the wetting features of decagonal quasicrystals. Using these materials, several properties have already been shown to be influenced by the periodic versus aperiodic order, such as optical

conductivity[62] or friction.[63] In this work, contact angles and interfacial energies were found to be comparable for the pseudo 10-fold $Al_5Co_2(2\bar{1}0)$ and the $Al_5Co_2(001)$ surfaces (Tables 1 and 2). Here, we only considered an hexagonal-like interfacial structure for both orientations. While the interfacial structure adopted for $Al_5Co_2(001)$ may be the lowest energy configuration (a pseudogap is visible in the density of states, suggesting a pseudomorphic-like structure), no pseudogap is noticeable for $Al_5Co_2(2\bar{1}0)$, suggesting that a more realistic interface may lead to a smaller contact angle. It is indeed fulfilled by considering the $P_{B\text{-}4Co}$ model for $Al_5Co_2(2\bar{1}0)$ (Table S5). However, from the knowledge gained by the analysis of $Pb/Al_{13}Co_4(100)$, no drastic difference ($\Delta\theta > 35°$) is anticipated. We may then predict that the wetting anisotropy is rather small using quasicrystalline approximants, similarly to what was observed for simple metal/metal interfaces.[64]

Here, electronic interactions at the interface play a significant role. When dealing with two metals, such as Pb(111)/Al(111), the bonding at the interface is metallic, as illustrated by the DOS calculations (Figure 5). A slight charge transfer occurs (Table S6), not influenced by the thickness of the Pb adlayer, resulting from the small electronegativity difference between Al and Pb (1.61 and 1.87, respectively[65]). It leads to a rather high interaction energy ($E^{interaction}_{Pb/Al(111)}$ = 65.7 meV/Å^2), defined as $E^{interaction}_{Pb/substrate} = -E^{tot}_{Pb/substrate} + E^{tot}_{substrate} + E^{tot}_{Pb}$, where $E^{tot}_{Pb/substrate}$, $E^{tot}_{substrate}$, and E^{tot}_{Pb} are the total energies of the substrate covered with a lead single layer, the clean substrate, and a free-standing Pb adlayer. The good wetting observed for this system can then be attributed to this strong interaction.

When dealing with Pb deposited on the complex Al−Co intermetallic surfaces, the effect of the interface extends further into the intermetallic compound. Indeed, the Co d-states on the subinterface now participate in the charge distribution (Table S6) and in orbital hybridization with the Pb sp-states (Figure 5). The interaction between the Pb adlayer and the substrate remains metallic but with a non-negligible iono-covalent character. Interfacial Al atoms behave as donor atoms (Figure 6): the Bader charges carried by surface Al atoms

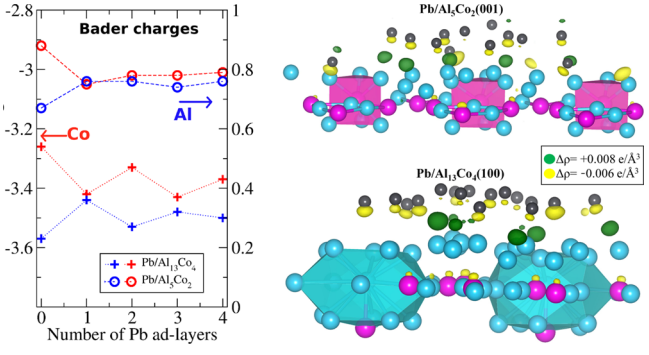

Figure 6. Bader charges for interfacial Al and Co atoms, as a function of the number of Pb adlayers. Charge density deformation at the $Pb/Al_{13}Co_4(100)$ and $Pb/Al_5Co_2(001)$ interfaces.

increase from 0.23*e* and 0.67*e* for the clean $Al_{13}Co_4(100)$ and $Al_5Co_2(001)$ surfaces, respectively, to 0.36*e* and 0.76*e* for the surfaces covered with Pb, on average (Table S6, Figure 6). This leads to a charge transfer toward interfacial Pb (ΔQ_{Pb} = −0.06*e*) and subsurface Co atoms. The Bader charges carried by subsurface Co atoms decrease from −3.26*e* and −2.92*e* for the clean $Al_{13}Co_4(100)$ and $Al_5Co_2(001)$ surfaces, respectively, to −3.42*e* and −3.05*e* for the surfaces covered with Pb, on average. The resulting interaction energy is rather large: $E^{interaction}_{Pb/Al_{13}Co_4(100)}$ = 80.5 meV/Å^2 and $E^{interaction}_{Pb/Al_5Co_2(001)}$ = 93.2 meV/Å^2. Such strong interactions however lead to a poor wetting behavior, demonstrating that the consideration of the interaction energy alone cannot explain our results.

Wetting is a tricky property which depends on the interfacial energy between the substrate and the liquid as well as on the surface energies of the substrate and the liquid. The factor $\Delta\gamma = \gamma^{substrate}_{modified} - \gamma_{interface}$ is calculated to be positive for good wetting systems (+15 meV/Å^2 for Al(111)) and slightly negative for the Al−Co complex intermetallics (−1 meV/Å^2 for $Al_{13}Co_4(100)$, −3 meV/Å^2 for $Al_5Co_2(001)$, and −1 meV for $Al_5Co_2(2\bar{1}0)$). However, the calculation of such a factor is not straightforward.

Electronic density of states at the Fermi energy ($n(E_F)$) is a key factor in condensed matter physics and material science that determines the properties of metals. It has already been shown to drive the wetting properties of Cu deposited on different oxides.[66] The partial electronic density of states within the bulk material (n^{3p}_{Al}) has also been invoked to analyze the unique reversible adhesion energy of water on several Al-based intermetallics.[21] Surface energies are derived from $n(E_F)$,[67−70] within the free electron model, while interfacial energies depend on the work function differences ΔW between the two metals. The latter is small for low electron density metals ($\Delta W_{Al(111)/Pb(111)}$ < 0.1 eV, $W_{Al(111)}$ = 3.85 eV (our work) and $W_{Pb(111)}$ = 3.78 eV[71]), because the electronic transfer is facile between two metals. It is larger when considering the interface between lead and complex intermetallic compounds with small $n(E_F)$ ($W_{Al_5Co_2(001)}$ = 4.02 eV and $W_{Al_{13}Co_4(100)}$ = 4.26 eV), leading to larger interfacial energies.[70] One then expects $\Delta\gamma > 0$ for small ΔW and $\Delta\gamma < 0$ for larger ΔW. Considering lead as a probe, good wetting is then expected for good metals, that is, presenting large $n(E_F)$, while poor wetting is predicted for compounds with small $n(E_F)$. It is in agreement with our observations: a small density of states at the Fermi energy corresponds to a larger value of the contact angle (Figure 7).

5. CONCLUSIONS

We reported the unexpected nonwetting behavior of liquid Pb metal droplets on two quasicrystalline approximants to decagonal quasicrystals, namely, Al_5Co_2 and $Al_{13}Co_4$. Thanks

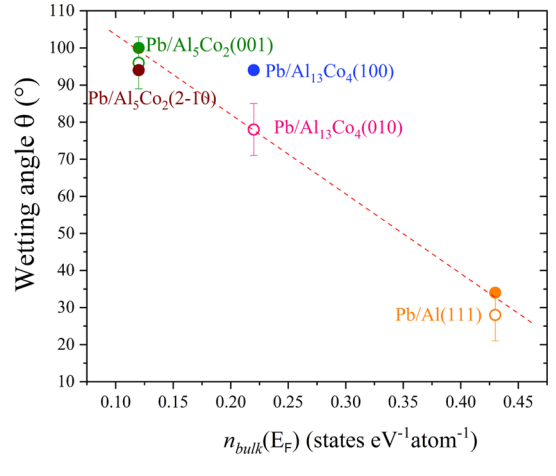

Figure 7. Contact angles plotted as a function of $n(E_F)$.

to our theoretical model based on the Young equation, the intrinsic wettability of Al−Co compounds is predicted from first-principles and validated by the good agreement with experimental measurements performed under a UHV by SEM.

The wetting properties have been discussed in terms of geometric and electronic effects. For Pb(111)/Al(111), the high-order commensurate $(\sqrt{31} \times \sqrt{31})R8.95°$ interface and the common pure metallic character of the two elements lead to good wetting. The situation is different for Pb(111)/Al_5Co_2(001), Pb(111)/$Al_5Co_2(2\bar{1}0)$, and Pb(111)/$Al_{13}Co_4$(100), even if the Al−Co compound surfaces present an Al-rich termination. In these systems, the contact angles are large (~90°). The intrinsic nonwettability can be directly assigned to electronic effects and correlated through the density of states at the Fermi energy.

In summary, we have developed an approach to predict the intrinsic surface Pb wettability of aluminum and two intermetallic compounds based on a simple DFT slab model. As compared with MD simulations based on empirical potentials, the proposed first principles method is much more efficient because fewer input parameters are required and a rather good accuracy, at least a better agreement with experimental observations, is obtained. Although we consider pure Al and Al−Co quasicrystalline approximants as a benchmark in this study, the proposed method is very general and may be applicable to any crystal surfaces and nonreactive metal liquids. This paves the way for a better fundamental understanding of wettability useful in a wide range of fields, such as catalysis for metal−support interactions.

■ ASSOCIATED CONTENT

Supporting Information

The Supporting Information is available free of charge at https://pubs.acs.org/doi/10.1021/acsami.9b20653.

Bulk and surfaces (thermodynamic results), Pb(111)/Al(111) (DOS and STM images), and Bader charges (PDF)

■ AUTHOR INFORMATION

Corresponding Author

Émilie Gaudry − *Université de Lorraine, CNRS, IJL, F-54000 Nancy, France;* orcid.org/0000-0001-6546-8323; Email: emilie.gaudry@univ-lorraine.fr

Authors

Kanika Anand − *Université de Lorraine, CNRS, IJL, F-54000 Nancy, France; CIRIMAT, Université de Toulouse, CNRS, INPT, UPS, 31030 Toulouse Cedex 4, France*

Vincent Fournée − *Université de Lorraine, CNRS, IJL, F-54000 Nancy, France;* orcid.org/0000-0001-5144-5075

Geoffroy Prévot − *Sorbonne Université, CNRS, Institut des NanoSciences de Paris, 75005 Paris, France*

Julian Ledieu − *Université de Lorraine, CNRS, IJL, F-54000 Nancy, France;* orcid.org/0000-0002-9896-0426

Complete contact information is available at: https://pubs.acs.org/10.1021/acsami.9b20653

Notes

The authors declare no competing financial interest.

■ ACKNOWLEDGMENTS

The authors thank Dr. M. Badawi for fruitful discussions about molecular dynamics calculations. We are very grateful to M.-C. de Weerd and our collaborators at the Ludwig Maximilians Universität (P. Gille's group) who provided several single crystals. We aknowledge support from the European Consortium ECMetAC and funding from the COMETE project (COnception in silico de Matériaux pour l'EnvironnemenT et l'Energie) co-funded by the European Union under the program "FEDER-FSE Lorraine et Massif des Vosges 2014-2020". This work was granted access to the High Performance Computing (HPC) resources of TGCC, CINES, IDRIS under the allocation 99642 attributed by GENCI (Grand Equipement National de Calcul Intensif). HPC resources were partially provided by the EXPLOR center hosted by Université de Lorraine (grant M4XXX0108).

■ REFERENCES

(1) Rosen, K. M.; Potash, M. L. Forty Years of Helicopter Ice Protection Experience At Sikorsky Aircraft. *J. Am. Helicopter Soc.* **1981**, *26*, 5−19.

(2) Ruan, M.; Li, W.; Wang, B.; Deng, B.; Ma, F.; Yu, Z. Preparation and Anti-icing Behavior of Superhydrophobic Surfaces on Aluminum Alloy Substrates. *Langmuir* **2013**, *29*, 8482−8491.

(3) Zuo, Z.; Liao, R.; Guo, C.; Yuan, Y.; Zhao, X.; Zhuang, A.; Zhang, Y. Fabrication and Anti-Icing Property of Coral-Like Superhydrophobic Aluminum Surface. *Appl. Surf. Sci.* **2015**, *331*, 132−139.

(4) Zhang, J.; Gu, C.; Tu, J. Robust Slippery Coating with Superior Corrosion Resistance and Anti-Icing Performance for AZ31B Mg Alloy Protection. *ACS Appl. Mater. Interfaces* **2017**, *9*, 11247−11257.

(5) Qing, Y.; Hu, C.; Yang, C.; An, K.; Tang, F.; Tan, J.; Liu, C. Rough Structure of Electrodeposition as a Template for an Ultrarobust Self-Cleaning Surface. *ACS Appl. Mater. Interfaces* **2017**, *9*, 16571−16580.

(6) Rahman, O. S. A.; Biswajyoti, M.; Aminul, I.; Keshri, A. Instant Tuning of Superhydrophilic to Robust Superhydrophobic and Self-Cleaning Metallic Coating: Simple, Direct, One-Step, and Scalable Technique. *ACS Appl. Mater. Interfaces* **2019**, *11*, 4616−4624.

(7) Feil, A. F.; Weibel, D. E.; Corsetti, R. R.; Pierozan, M. D.; Michels, A. F.; Horowitz, F.; Amaral, L.; Teixeira, S. R. Micro and Nano-Texturization of Intermetallic Oxide Alloys by a Single Anodization Step: Preparation of Artificial Self-Cleaning Surfaces. *ACS Appl. Mater. Interfaces* **2011**, *3*, 3981−3987.

(8) Wang, X.-Z.; Luo, H.; Muneshwar, T.; Fan, H.-Q.; Cadien, K.; Luo, J.-L. Zr_2N_2O Coating-Improved Corrosion Resistance for the Anodic Dissolution Induced by Cathodic Transient Potential. *ACS Appl. Mater. Interfaces* **2018**, *10*, 40111−40124.

(9) Xie, Z.-H.; Li, D.; Skeete, Z.; Sharma, A.; Zhong, C.-J. Nanocontainer-Enhanced Self-Healing for Corrosion-Resistant Ni Coating on Mg Alloy. *ACS Appl. Mater. Interfaces* **2017**, *9*, 36247−36260.

(10) Bi, C.; Wang, Q.; Shao, Y.; Yuan, Y.; Xiao, Z.; Huang, J. Non-Wetting Surface-Driven High-Aspect-Ratio Crystalline Grain Growth for Efficient Hybrid Perovskite Solar Cells. *Nat. Commun.* **2015**, *6*, 7747.

(11) Matteini, F.; Tütüncüoglu, G.; Potts, H.; Jabeen, F.; Fontcuberta i Morral, A. Wetting of Ga on SiO_x and Its Impact on GaAs Nanowire Growth. *Cryst. Growth Des.* **2015**, *15*, 3105−3109.

(12) Ray, N.; Froyen, L.; Vanmeensel, K.; Vleugels, J. Wetting and Solidification of Silver Alloys in the Presence of Tungsten Carbide. *Acta Mater.* **2018**, *144*, 459−469.

(13) Nautiyal, P.; Gupta, A.; Seal, S.; Boesl, B.; Agarwal, A. Reactive Wetting and Filling of Boron Nitride Nanotubes By Molten Aluminum During Equilibrium Solidification. *Acta Mater.* **2017**, *126*, 124−131.

(14) Li, L.; Cao, K.-Z.; Shen, P.; Jiang, Q.-C. Roles of Direct Current in Ultrafast Wetting of 3YSZ By $Sn_{3.0}Ag_{0.5}Cu$ and Joining To Ni. *Materialia* **2019**, *7*, 100399.
(15) Wang, S.; Liu, K.; Yao, X.; Jiang, L. Bioinspired Surfaces with Superwettability: New Insight on Theory, Design, and Applications. *Chem. Rev.* **2015**, *115*, 8230−8293.
(16) Su, B.; Tian, Y.; Jiang, L. Bioinspired Interfaces with Superwettability: From Materials to Chemistry. *J. Am. Chem. Soc.* **2016**, *138*, 1727−1748.
(17) Anastasiadis, S. H. Development of Functional Polymer Surfaces with Controlled Wettability. *Langmuir* **2013**, *29*, 9277−9290.
(18) Schlaich, C.; Wei, Q.; Haag, R. Mussel-Inspired Polyglycerol Coatings with Controlled Wettability: From Superhydrophilic to Superhydrophobic Surface Coatings. *Langmuir* **2017**, *33*, 9508−9520.
(19) Eustathopoulos, N. Wetting by Liquid Metals-Application in Materials Processing: the Contribution of the Grenoble Group. *Metals* **2015**, *5*, 350−370.
(20) Cui, Y.; Liang, F.; Yang, Z.; Xu, S.; Zhao, X.; Ding, Y.; Lin, Z.; Liu, J. Metallic Bond-Enabled Wetting Behavior at the Liquid Ga/$CuGa_2$ Interfaces. *ACS Appl. Mater. Interfaces* **2018**, *10*, 9203−9210.
(21) Dubois, J. M. A Model of Wetting On Quasicrystals in Ambient Air. *J. Non-Cryst. Solids* **2004**, *334-335*, 481−485.
(22) Dubois, J.-M. Properties and Applications of Quasicrystals and Complex Metallic Alloys. *Chem. Soc. Rev.* **2012**, *41*, 6760−6777.
(23) Bergman, C.; Girardeaux, C.; Perrin-Pellegrino, C.; Gas, P.; Dubois, J.-M.; Rivier, N. Contact Angles of Liquid Metals On Quasicrystals. *J. Phys.: Condens. Matter* **2008**, *20*, 314010.
(24) Bergman, C.; Girardeaux, C.; Perrin-Pellegrino, C.; Gas, P.; Chatain, D.; Dubois, J. M.; Rivier, N. Wetting of Decagonal $Al_{13}Co_4$ and Cubic AlCo Thin Films by Liquid Pb. *Philos. Mag.* **2006**, *86*, 849−854.
(25) Werder, T.; Walther, J. H.; Jaffe, R. L.; Halicioglu, T.; Noca, F.; Koumoutsakos, P. Molecular Dynamics Simulation of Contact Angles of Water Droplets in Carbon Nanotubes. *Nano Lett.* **2001**, *1*, 697−702.
(26) Weijs, J. H.; Snoeijer, J. H.; Lohse, D. Formation of Surface Nanobubbles and the Universality of Their Contact Angles: A Molecular Dynamics Approach. *Phys. Rev. Lett.* **2012**, *108*, 104501.
(27) Reguera, J.; Ponomarev, E.; Geue, T.; Stellacci, F.; Bresme, F.; Moglianetti, M. Contact Angle and Adsorption Energies of Nanoparticles At the Air−Liquid Interface Determined By Neutron Reflectivity and Molecular Dynamics. *Nanoscale* **2015**, *7*, 5665−5673.
(28) Shi, Z.; Lowekamp, J. B.; Wynblatt, P. Energy of the Pb(111)|| Al(111) Interface. *Metall. Mater. Trans.* **2002**, *33*, 1003−1007.
(29) Landa, A.; Wynblatt, P.; Johnson, E.; Dahmen, U. Computer Simulation of Pb/Al Interfaces. *Acta Mater.* **2000**, *48*, 2557−2563.
(30) Zhao, Z.-Y.; Li, T.; Duan, Y.-R.; Wang, Z.-C.; Li, H. Wetting and Coalescence of the Liquid Metal On the Metal Substrate. *Chin. Phys. B* **2017**, *26*, 083104.
(31) Meier, M.; Ledieu, J.; Weerd, M.-C. D.; Huang, Y.-T.; Abreu, G. J. P.; Diehl, R.; Mazet, T.; Fournée, V.; Gaudry, E. Interplay Between Bulk Atomic Clusters and Surface Structure in Complex Intermetallic Compounds: the Case Study of the $Al_5Co_2(001)$ Surface. *Phys. Rev. B: Condens. Matter Mater. Phys.* **2015**, *91*, 085414.
(32) Gille, P.; Bauer, B. Single Crystal Growth of $Al_{13}Co_4$ and $Al_{13}Fe_4$ from Al-rich Solutions by the Czochralski Method. *Cryst. Res. Technol.* **2008**, *43*, 1161−1167.
(33) Shin, H.; Pussi, K.; Gaudry, É.; Ledieu, J.; Fournée, V.; Alarcón-Villaseca, S.; Dubois, J.-M.; Grin, Y.; Gille, P.; Moritz, W.; Diehl, R. Structure of the Orthorhombic $Al_{13}Co_4(100)$ Surface Using LEED, STM and Ab Initio Studies. *Phys. Rev. B: Condens. Matter Mater. Phys.* **2011**, *84*, 085411.
(34) Blöchl, P. E. Projector Augmented-Wave Method. *Phys. Rev. B: Condens. Matter Mater. Phys.* **1994**, *50*, 17953−17979.
(35) Kresse, G.; Joubert, D. From Ultrasoft Pseudopotentials To the Projector Augmented-Wave Method. *Phys. Rev. B: Condens. Matter Mater. Phys.* **1999**, *59*, 1758−1775.
(36) Monkhorst, H. J.; Pack, J. D. Special Points for Brillouin-Zone Integrations. *Phys. Rev. B: Condens. Matter Mater. Phys.* **1976**, *13*, 5188−5192.
(37) Perdew, J. P.; Burke, K.; Ernzerhof, M. Generalized Gradient Approximation Made Simple. *Phys. Rev. Lett.* **1996**, *77*, 3865.
(38) Perdew, J. P.; Burke, K.; Ernzerhof, M. Generalized Gradient Approximation Made Simple [Phys. Rev. Lett. 77, 3865 (1996)]. *Phys. Rev. Lett.* **1997**, *78*, 1396.
(39) Scheid, P.; Chatelier, C.; Ledieu, J.; Fournée, V.; Gaudry, É. Bonding Network and Stability of Clusters: The Case Study of the $Al_{13}TM_4$ Pseudo-10fold Surfaces. *Acta Crystallogr., Sect. A: Found. Adv.* **2019**, *75*, 314−324.
(40) Meier, M.; Ledieu, J.; Fournée, V.; Gaudry, É. Semi-Hydrogenation of Acetylene On Al_5Co_2 Surfaces. *J. Phys. Chem. C* **2017**, *121*, 4958−4969.
(41) Kandaskalov, D.; Fournée, V.; Ledieu, J.; Gaudry, É. Catalytic Semihydrogenation of Acetylene on the (100) Surface of the o-$Al_{13}Co_4$ Quasicrystalline Approximant: Density Functional Theory Study. *J. Phys. Chem. C* **2017**, *121*, 18738−18745.
(42) Burkhardt, U.; Ellner, M.; Grin, Y.; Baumgartner, B. Powder Diffraction Refinement of the Co_2Al_5 Structure. *Powder Diffr.* **1998**, *13*, 159−162.
(43) Grin, J.; Burkhardt, U.; Ellner, M.; Peters, K. Crystal Structure of Orthorhombic Co_4Al_{13}. *J. Alloys Compd.* **1994**, *206*, 243−247.
(44) Meier, M.; Ledieu, J.; Weerd, M.-C. D.; Fournée, V.; Gaudry, E. Structural Investigations of $Al_5Co_2(2\bar{1}0)$ and (100) Surfaces: Influence of Bonding Strength and Annealing Temperature On Surface Terminations. *Phys. Rev. B* **2016**, *93*, 075412.
(45) Gaudry, É.; Chatelier, C.; McGuirk, G.; Loli, L. S.; DeWeerd, M.-C.; Ledieu, J.; Fournée, V.; Felici, R.; Drnec, J.; Beutier, G.; de Boissieu, M. Structure of the $Al_{13}Co_4(100)$ Surface: Combination of Surface X-Ray Diffraction and Ab Initio Calculations. *Phys. Rev. B* **2016**, *94*, 165406.
(46) Fournée, V.; Ledieu, J.; Gaudry, E.; de Weerd, M.-C.; Diehl, R. D. The (100) Surface of the $Al_{13}Co_4$ Quasicrystalline Approximant. *MRS Proc.* **2013**, *1517*, mrsf12-1517-kk02-07.
(47) Jiang, H.; Patel, A. J. Recent Advances in Estimating Contact Angles Using Molecular Simulations and Enhanced Sampling Methods. *Curr. Opin. Chem. Eng.* **2019**, *23*, 130−137.
(48) Lu, J. Y.; Ge, Q.; Li, H.; Raza, A.; Zhang, T. Direct Prediction of Calcite Surface Wettability with First-Principles Quantum Simulation. *J. Phys. Chem. Lett.* **2017**, *8*, 5309−5316.
(49) Dupré, A. *Théorie Mécanique de la Chaleur*; Gauthier-Villars: Paris, 1869.
(50) Young, T. An Essay on the Cohesion of Fluids. *Philos. Trans. R. Soc. London* **1805**, *95*, 65−87.
(51) Schwaneke, A. E.; Falke, W. L. Surface Tension and Density of Liquid Lead. *J. Chem. Eng. Data* **1972**, *17*, 291−293.
(52) Jank, W.; Hafner, J. Structural and Electronic Properties of the Liquid Polyvalent Elements: the Group-IV Elements Si, Ge, Sn, and Pb. *Phys. Rev. B: Condens. Matter Mater. Phys.* **1990**, *41*, 1497−1515.
(53) Bombis, C.; Emundts, A.; Nowicki, M.; Bonzel, H. P. Absolute Surface Free Energies of Pb. *Surf. Sci.* **2002**, *511*, 83−96.
(54) Deniozou, T.; Ledieu, J.; Fournée, V.; Wu, D.; Lograsso, T. A.; Li, H. T.; Diehl, R. D. Aperiodic and Modulated Pb Thin Films on Fivefold Icosahedral Al-Cu-Fe and Al(111): Tailoring the Structure of Pb. *Phys. Rev. B: Condens. Matter Mater. Phys.* **2009**, *79*, 245405.
(55) Villaseca, S. A.; Dubois, J.-M.; Gaudry, É. Lead Adsorption On the Pseudo-Tenfold Surface of the $Al_{13}Co_4$ Complex Metallic Alloy: A First Principle Study. *Int. J. Quantum Chem.* **2013**, *113*, 840−846.
(56) Addou, R.; Shukla, A. K.; Alarcón-Villaseca, S.; Gaudry, É.; Deniozou, T.; Heggen, M.; Feuerbacher, M.; Widmer, R.; Gröning, O.; Fournée, V.; Dubois, J.-M.; Ledieu, J. Lead Adsorption on the $Al_{13}Co_4$ (100) Surface: Heterogeneous Nucleation and Pseudomorphic Growth. *New J. Phys.* **2011**, *13*, 103011.
(57) Villaseca, S. A.; Loli, L. S.; Ledieu, J.; Fournée, V.; Gille, P.; Dubois, J.-M.; Gaudry, E. Oxygen Adsorption on the $Al_9Co_2(001)$ Surface: First-Principles and STM Study. *J. Phys.: Condens. Matter* **2013**, *25*, 355003.

(58) Anand, K. Surface Properties of Complex Intermetallics at the Nanoscale : from Fundamentals to Applications. Ph.D. Thesis, University Lorraine, 2018.
(59) Krajčí, M.; Hafner, J.; Ledieu, J.; Fournée, V.; McGrath, R. Quasiperiodic Pb Monolayer on the Fivefold *i*-Al-Pd-Mn Surface: Structure and Electronic Properties. *Phys. Rev. B: Condens. Matter Mater. Phys.* **2010**, *82*, 085417.
(60) Lange, B.; Posner, R.; Pohl, K.; Thierfelder, C.; Grundmeier, G.; Blankenburg, S.; Schmidt, W. G. Water Adsorption on Hydrogenated Si(111) Surfaces. *Surf. Sci.* **2009**, *603*, 60−64.
(61) Carchini, G.; García-Melchor, M.; Łodziana, Z.; López, N. Understanding and Tuning the Intrinsic Hydrophobicity of Rare-Earth Oxides: A DFT+U Study. *ACS Appl. Mater. Interfaces* **2016**, *8*, 152−160.
(62) Basov, D. N.; Timusk, T.; Barakat, F.; Greedan, J.; Grushko, B. Anisotropic Optical Conductivity of Decagonal Quasicrystals. *Phys. Rev. Lett.* **1994**, *72*, 1937.
(63) Park, J. Y.; Ogletree, D. F.; Salmeron, M.; Ribeiro, R. A.; Canfield, P. C.; Jenks, C. J.; Thiel, P. A. High Frictional Anisotropy of Periodic and Aperiodic Directions on a Quasicrystal Surface. *Science* **2005**, *309*, 1354.
(64) Chatain, D.; Métois, J. J. A New Procedure for the Determination of the Free Energies of Solid-Fluid Interfaces From the Anisotropy of Wetting of A Melt On Its Solid. *Surf. Sci.* **1993**, *291*, 1−13.
(65) *CRC Handbook of Chemistry and Physics*, Haynes, W. M., Ed.; CRC Press/Taylor and Francis: Boca Raton, USA, 1996.
(66) Eustathopoulos, N.; Nicholas, M.; Drevet, B. *Wettability at High Temperatures*; Pergamon Press: Amsterdam-Lausanne-New-York-Oxford-Shannon-Singapore-Tokyo, 1999.
(67) Lang, N. D.; Kohn, W. Theory of Metal Surfaces: Charge Density and Surface Energy. *Phys. Rev. B: Condens. Matter Mater. Phys.* **1970**, *1*, 4555−4568.
(68) Lang, N. D.; Kohn, W. Theory of Metal Surfaces: Work Function. *Phys. Rev. B: Condens. Matter Mater. Phys.* **1971**, *3*, 1215−1223.
(69) Muscat, J. P.; Allan, G. Interface Energy of Two Free-Electron-Like Metals. *J. Phys. F: Met. Phys.* **1977**, *7*, 999−1008.
(70) Wu, B.; Zhang, Z. Stability of Metallic Thin Films Studied with a Free Electron Model. *Phys. Rev. B: Condens. Matter Mater. Phys.* **2008**, *77*, 035410.
(71) Yu, D.; Scheffler, M. First-Principles Study of Low-Index Surfaces of Lead. *Phys. Rev. B: Condens. Matter Mater. Phys.* **2004**, *70*, 155417.